Hole Expansion Simulations of TWIP Steel Sheet Sample

L. Xu, L. Chen, D. Steglich, B. C. Decooman, and F. Barlat

Citation: AIP Conference Proceedings **1252**, 1271 (2010); doi: 10.1063/1.3457529
View online: http://dx.doi.org/10.1063/1.3457529
View Table of Contents: http://scitation.aip.org/content/aip/proceeding/aipcp/1252?ver=pdfcov
Published by the AIP Publishing

Hole Expansion Simulations of TWIP Steel Sheet Sample

L. Xu[a], L. Chen[b], D. Steglich[a, c], B. C. Decooman[b] and F. Barlat[a]

[a]*Materials Mechanics Laboratory, Graduate Institute of Ferrous Technology, Pohang University of Science and Technology, Pohang, 790-784, Korea*
[b]*Materials Design Laboratory, Graduate Institute of Ferrous Technology, Pohang University of Science and Technology, Pohang, Korea*
[c]*Materials Mechanics, GKSS Research Centre ,Geesthacht, Germany*

Abstract. In this work, the stretch flangeability of a TWIP steel sheet sample was investigated both experimentally and numerically through the hole expansion test. Uniaxial tension and disk compression tests were performed to characterize the flow behavior and plastic anisotropy for the TWIP steel sheet sample. The punch load-stroke curve, hole diameter and specimen surface strain distribution near the hole was measured. Then finite element simulations of the hole expansion test were carried out using the finite element code ABAQUS with three yield criteria: von Mises, Hill 1948 and Yld2000-2d. The predicted and experimental results were compared in terms of the final hole radii and the strain distribution.

Keywords: TWIP steel, Hole expansion, Finite element, Stretch flangeability
PACS: 62.20.f

INTRODUCTION

Advanced high strength steels (AHSS) have been continuously improved to meet the various requirements of the automotive industry, such as vehicle weight containment, crash performance improvement, energy saving considerations and environmental protection. Generally, these AHSS exhibit high strength and, for some, excellent ductility in the uniaxial tension. However, issues usually hidden in lower strength steels tend to appear in AHSS. In particular, premature ductile fracture occurring in stretch-flanging processes, such as hub hole forming for automotive wheels, has been observed [1]. Conventional approaches to assess formability such as the forming limit diagram are not sufficient to describe the ductility and fracture behaviour in stretch-flanging [2]. The hole expansion test has been recognized as a discriminating method to characterize the forming behaviour in stretch-flanging processes. Therefore, it is important to accurately analyze the deformation behavior and fracture of AHSS in the hole expansion test.

Experimental investigations and finite element simulations of the hole expansion test were performed for a high Mn TWIP steel sheet sample. The basic mechanical properties of this material were characterized using the uniaxial tension and disk compression tests. The finite element simulations were performed using the commercial finite element code ABAQUS. Three different yield criteria, von Mises [3], Hill 1948 [4] and Yld2000-2d [5], were used in the simulations to study the influence of plastic anisotropy. Experimental and numerical results were compared in order to identify the main parameters controlling stretch-flangeability of this material.

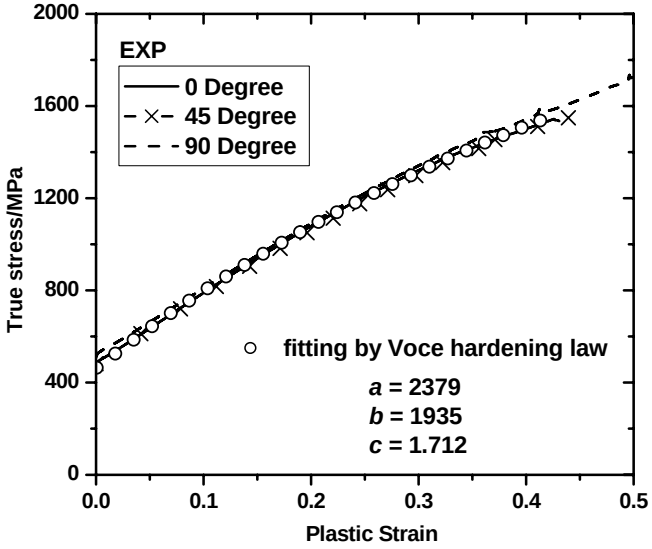

FIGURE 1. The stress-strain curves of the TWIP steel sheet sample.

TABLE 1. Normalized flow stresses at the amount of plastic work per unit volume w = 5 MPa and r values

	0˚	**45˚**	**90˚**	**biaxial**
flow stress	1.000	1.016	1.066	1.125
r value	0.79	1.13	1.28	0.64

EXPERIMENTAL

Uniaxial Tension Test

Standard uniaxial tensile tests were conducted to determine monotonic stress-strain curves and r values of the TWIP steel sheet sample. The tests were performed using standard specimens at a strain rate of 0.001/s on ZWICK/Roell Z100 tension tester. Three specimens were deformed in each of the three directions, namely 0˚, 45˚, 90˚ from the rolling direction (RD). The stress-strain curves are shown in Fig. 1. The stress-strain curve measured in the RD was chosen as the reference stress-strain curve for this material. It was approximated by a Voce hardening law, Equation (1), also shown in Fig. 1.

$$\bar{\sigma} = a - bEXP\left(-c\bar{\varepsilon}\right) \tag{1}$$

In the equation, $\bar{\sigma}$ and $\bar{\varepsilon}$ represent the effective stress and strain, respectively, a, b and c are the hardening coefficients.

Representative flow stresses were obtained for each loading direction at the amount of plastic work per unit volume of $w = 5$ *MPa.* This value corresponds roughly to plastic strain of 0.01 in uniaxial tension. All stresses were normalized by the uniaxial stress obtained in the RD. r values were calculated up to the engineering strain of 30%, and they keep constant in the range. These normalized flow stresses and r values are listed in Table 1.

Disk Compression Test

The through thickness disk compression tests [3, 6] were performed on a Gleeble 3500 tester to obtain the plastic anisotropy in the balanced biaxial tension stress state. Many different lubricants and surface conditions were tried in the experiments [6]. Several samples with 1.25 mm thickness and 5.0 mm diameter were compressed through the sheet normal direction (ND). The biaxial r value (r_b) was determined as the ratio of transverse strains to the rolling strains after through thickness compression up to the thickness strain of 0.5. The average r_b value from all the disk

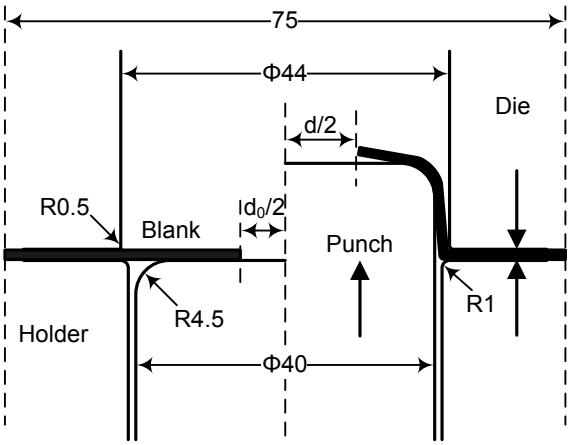

FIGURE 2. Experimental schematic of hole expansion test (dimension: mm).

compression tests is listed in Table 1. The balanced biaxial stresses at the amount of plastic work per unit volume $w = 5$ MPa were obtained from the compressive load, assuming that the plastic deformation is independent of hydrostatic pressure. Since all the stresses are upper bounds due to the friction effects, the lowest stress was considered as a rough estimate of the real balanced biaxial stress.

Hole Expansion Test

An Erichsen hydraulic sheet metal tester with 600 kN capacity was used to perform the flat bottom hole expansion tests. A schematic view of the test is shown in Fig. 2. During the test, the specimen with a central hole was firstly clamped between the lower blank holder and the upper die. The draw-in of the outer sample periphery was prevented by means of a high constant blank holder force of 65 KN. Then, the punch force was applied with the velocity of 20 mm/min. Once the punch force suddenly dropped due to the appearance of a radial crack, the test was stopped. It is well known that the stretch flangeability of the material is reduced significantly by the burrs, edge damage and residual stresses resulting from hole punching [7]. Therefore, a burr-free, high quality drilled surface edge finish was used to form the hole of the specimen in this work. The initial hole diameter d_0 was 12 mm. After the test, the diameter of the deformed hole, d, was measured along the circumference.

During the hole expansion test, in-situ strain analysis in the specimen surface was carried out using an AutoGrid optical system. This allowed monitoring the strain path for each point in the vicinity of the hole. For this, the specimens were etched with a 1 mm square grid pattern before the test. Four CCD cameras, set up above the sheet tester, recorded the distortion of the grid and monitored the local strains continuously during the tests.

CONSTITUTIVE MODEL

To predict the plastic behaviour of the TWIP steel sheet sample, simulations were performed with three yield criteria, von Mises, Hill 1948 and Yld2000-2d. Von Mises represented the isotropic case, while Hill 1948 and Yld2000-2d were used to describe plastic anisotropy. The input data needed to determine the anisotropy coefficients for Hill 1948 were the r values at 0°, 45°, 90° from the RD, and the uniaxial yield stress in the RD. For Yld2000-2d, the coefficients were calculated from the uniaxial stresses and r values at 0°, 45°, 90° from the RD, the balanced biaxial stress and r value, r_b. Because the TWIP steel has the fully austenitic microstructure, the exponent of Yld2000-2d was set to 8 as recommended for FCC crystal structures [8].

The experimental and predicted flow stresses at the plastic work per unit value of 5 MPa and r values from the different yield criteria are shown in Fig. 3. The figure shows that, among the three yield criteria, Yld2000-2d can fit experimental data best for both the flow stresses and r values. Hill 1948 and von Mises cannot capture the flow stresses in all directions accurately. This is because the flow stresses in the directions other than RD, are not required for determining Hill 1948 and von Mises yield criteria, as explained before. Figure 4 shows the experimental yield points and the yield loci predicted with the three yield criteria. As shown in the figures, compared with the

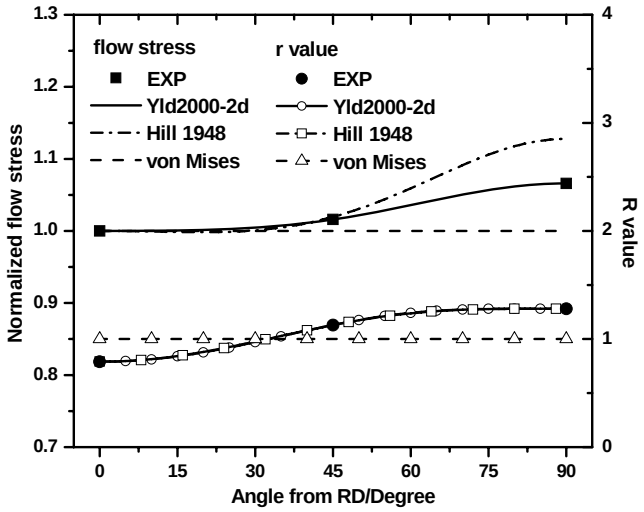

FIGURE 3. Experimental and predicted normalized flow stresses at plastic strain of 1% and *r* values.

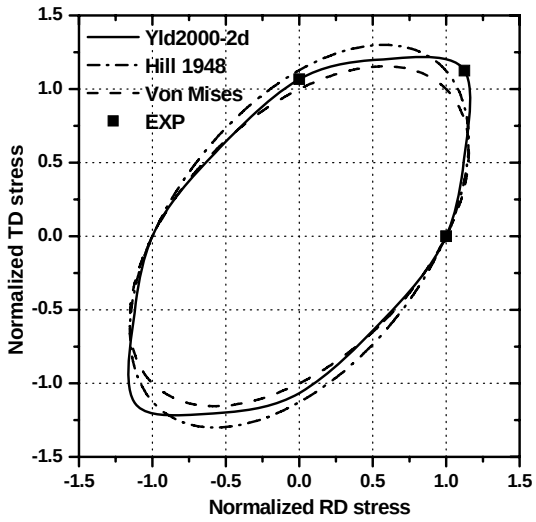

FIGURE 4. Experimental and predicted yield loci using different yield criteria.

experimental results, Hill 1948 yield function overestimated the uniaxial tension stress in the transverse direction (TD) and underestimated the balanced biaxial stress. Von Mises underestimated both of them while Yld2000-2d accurately captured all the experimental data. Therefore, it can be concluded that Yld2000-2d criterion can predict plastic anisotropy the most accurately among the three yield criteria.

FINITE ELEMENT MODEL

Finite element simulations of the hole expansion test were performed using ABAQUS/Standard. Only one quarter of the specimen was analyzed due to the orthotropic symmetry of the material and the full symmetry of the process itself. 4-node shell elements with reduced integration (S4R) and 5 integration points in the thickness direction were used for the specimen. 20 and 38 elements were used in the circumferential and radial directions, respectively. The punch, die and blank holder were defined as rigid analytical surfaces. The model is visualized in Fig. 5.

Node-to-surface contact formulation was used to describe the interaction between sheet and punch, sheet and holder and sheet and die, respectively. Between sheet, holder and die, no tangential motion is observed in the

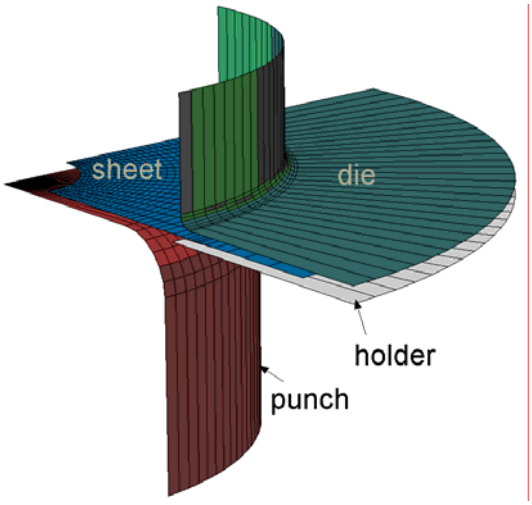

FIGURE 5. Finite element quarter-model for the hole expansion simulation.

experiment. Thus, the displacement of the sheet in the clamped region was suppressed in the simulations by respective boundary conditions. Between sheet and punch, tangential stresses are produced due to Coulomb friction. The corresponding coefficient was calibrated using the punch load-stroke curve as explained below.

The simulation of the experiments was split into two stages, namely the forming operation corresponding to the punch moving upward and the unloading phase (springback) representing the disassembling of the specimen from the testing equipment. Since the experimental punch velocity was used in the simulation, the strain rates in the simulation were identical to those of the experiments. As both stages of the simulation are full implicit, no mass scaling had to be used.

The constitutive behaviour of the material was assumed to be elastic-plastic, with isotropic, rate-independent hardening and the different yield criteria, von Mises, Hill 1948 and Yld2000-2d, as mentioned in Section 3.

RESULTS AND DISCUSSION

Figure 6(a) shows the experimental and numerical punch force when the punch stroke increases from 0 to 10 mm during the hole expansion. When the friction coefficient between the punch and the specimen was 0.06, the numerical load-stroke curves from the three yield criteria were in agreement with the experiment. Therefore, in terms of the punch force, it cannot be determined which yield criterion is the best to simulate the hole expansion test. In addition, among the numerical results, the punch force from Hill 1948 theory is always the highest and that from von Mises is always the lowest. This order of the punch force levels might be explained by the size of the predicted yield surfaces shown in Fig. 4. It is known that the specimen during the hole expansion process is deformed in the biaxial tension stress state. Fig. 4 demonstrates that, in the biaxial tension region, from TD uniaxial stress state to balanced biaxial stress state, the normalized stresses from Hill 1948 are higher than those from von Mises and Yld2000-2d criteria. Moreover, von Mises leads to the smallest normalized yield locus.

Fig. 6(b) represents the numerical evolution of the hole radius in the RD and strain rates at the same position as computed with Yld2000-2d yield function. When the punch stroke becomes larger, the hole radius increases more rapidly. The numerical hole radii with other yield criteria have the similar trend but result in slightly different final values. In terms of the strain rate, the absolute values in both directions also increase as the punch moves forward. It reached to 0.1 in the circumferential direction and -0.05 in the radial direction. This means the experimental results could be affected by the strain rate, since it is known than the TWIP steel exhibits the negative strain rate sensitivity. However, the effect is not considered in the simulations.

Figure 7(a) shows the experimental and numerical hole radii along the hole circumference at the punch stroke of about 10 mm, right before the specimen fractured in the experiment. They were normalized by the initial hole radius 6 mm. As shown in the figure, no matter which yield criterion was used in the simulation, the numerical hole radii are generally higher than experimental radii in all the directions of the hole periphery. In particular, the difference between the experimental radii and those of the simulation with Yld2000-2d reaches up to about 16%, which is the largest deviation between experimental and numerical results. It is worth noticing that the simplest yield criterion,

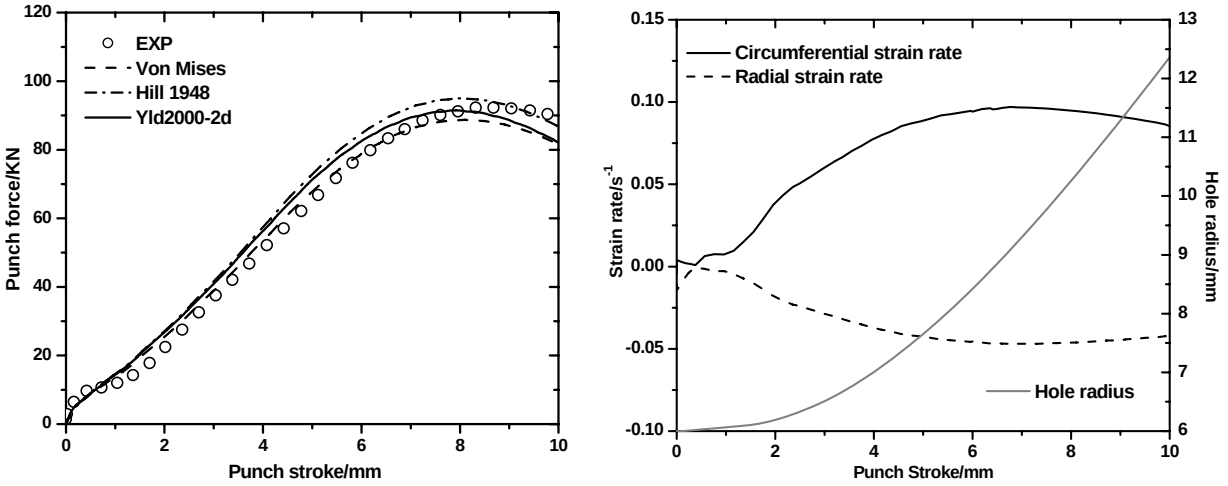

(a) (b)

Figure 6. Experimental and numerical punch force (a), numerical hole radius and strain rate (b) with the increase of punch stroke.

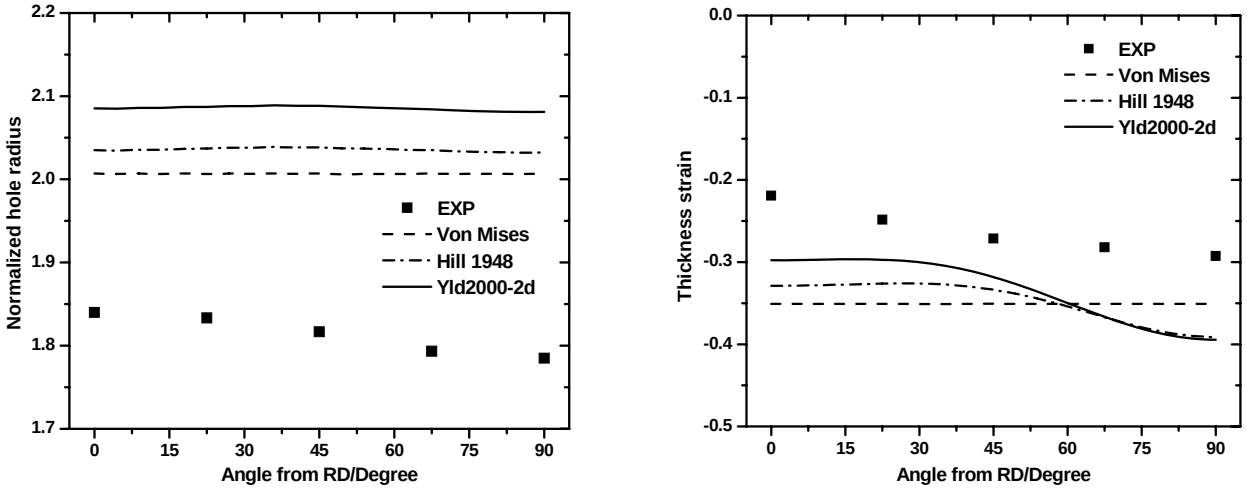

(a) (b)

Figure 7. Normalized hole radius (a) and thickness strain (b) at the punch stroke of about 10 mm.

von Mises, leads to the best predicted values but the difference is still about 10%. This difference might be due to the fact that the experimental hole radii were measured after a crack appeared along the radial direction. It is known that the existence of the crack affects the hole radii.

In terms of the plastic anisotropy, that is to say, the difference of hole radii along the circumference, none of the yield criteria can predict the experimental trends. In the experiment, the maximum hole radius occurs in the RD and the minimum does in the TD. This seems to correlate with the *r* value, which gradually increases from the RD to the TD as shown in Fig. 3. The experimental difference between the maximum and minimum hole radii is about 3%, while the numerical value is 0.5% for Yld2000-2d and 0.3% for Hill 1948. Therefore, more work is needed to understand more deeply the variations of the hole radii. Moreover, it is worth pointing out that, although the hole was formed by a high-quality drilled finish, the micro-defects still exist along the hole edge, which can induce stress concentration and inhomogeneity of the deformation. Of course, the simulations can not capture this feature. This also could be the reason for the difference between the experimental and numerical hole radii.

Experimental and numerical thickness strain along the hole circumference at the punch stroke of about 10 mm is shown in Fig. 7(b). It can be found that some discrepancy of thickness strain exists between the experiment and the simulations. Since the numerical hole radii at the same time are larger than those in the experiment, it is expected that the numerical thickness strains are smaller than those from the experiments. In terms of the variation of thickness strain along the hole periphery, although the predicted tendency with both anisotropic yield functions did not match the experimental one well, it seems that the difference between the maximum and minimum thickness

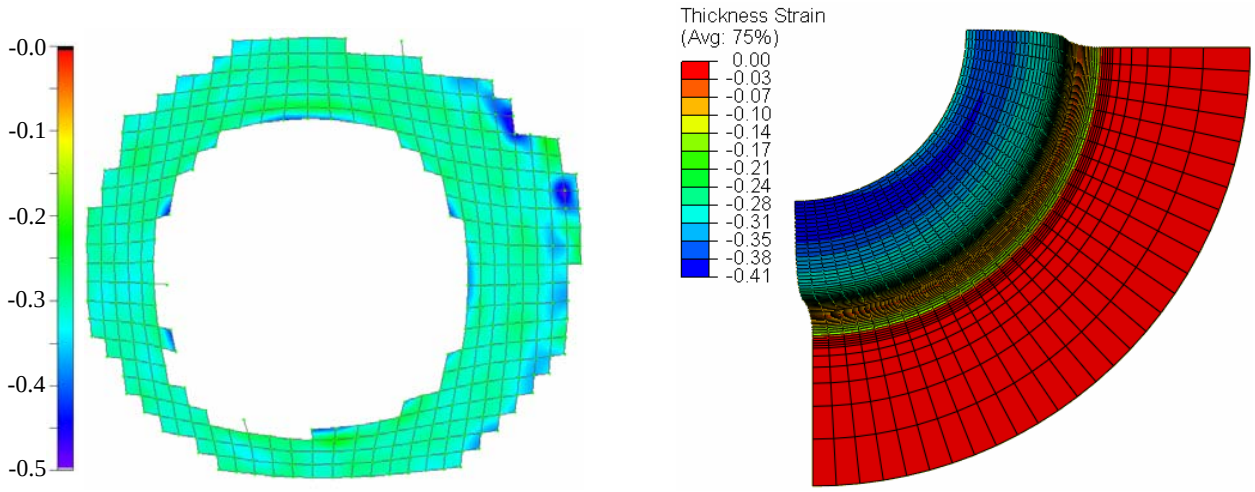

(a) (b)

Figure 8. Thickness strain distribution of the specimen at the punch stroke of about 10 mm: experiment (a); simulation with Yld2000-2d (b).

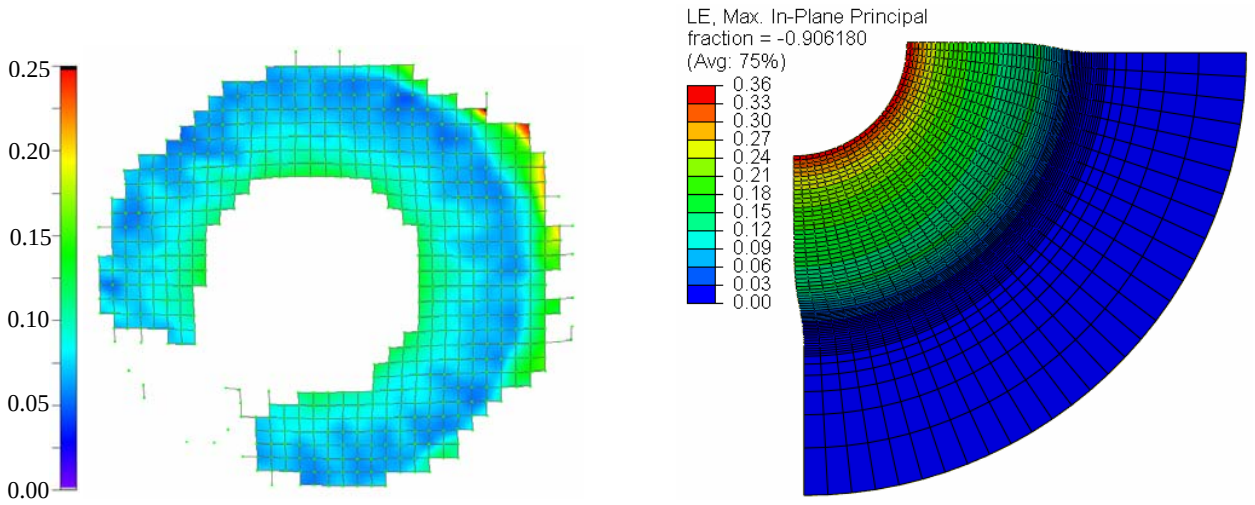

(a) (b)

Figure 9. Major principal strain at the punch stroke of about 6 mm: (a) experiment; (b) simulation with Yld2000-2d.

strains can be predicted. The experimental value is about 0.08 and the numerical value is close to 0.1 for Yld2000-2d and 0.08 for Hill 1948.

Figure 8 shows the thickness strain distribution from the experiment (a) and the simulation with Yld2000-2d yield criterion (b) at the punch stroke of about 10 mm. It was demonstrated in Fig. 8(a) that there is almost no thickness gradient from the hole edge to the punch shoulder in the experiment. The blue part from the simulation in Fig. 8(b) represents the same region as the experiment in Fig. 8(a). Although, in this part, a slight strain gradient was observed, it still can be concluded that the thickness strain distribution was nearly homogenous from hole edge to punch shoulder in the simulation. This phenomenon also exists at other steps of the deformation in both the experiments and simulations. Moreover, the experiment and the simulations lead to different thickness strains from the hole edge to the punch shoulder, about 0.3 for the former and about 0.4 for the latter. This corresponds to what is shown in Fig. 7(b) and can be explained in the same way. The discrepancy between the experiments and simulations is not the same with different yield criteria.

Due to the effect of the radial crack, it might be interested to investigate the results before reaching the maximum punch force. Figure 9 shows the major principal (circumferential) strain distribution at the punch stroke of 6 mm in the experiment (a) and the simulation with Yld2000-2d yield criterion (b). In Fig. 9(a), the major strain around the hole edge is about 0.15, while this value in the simulation shown in Fig. 9(b) is over 0.3. Therefore, it can be

expected from the result that the hole radii from the simulation would be larger than that in the experiment even before the maximum force is reached, and the thickness strain is in contrast.

CONCLUSION

In this work, uniaxial tension, disk compression and hole expansion tests were performed to investigate the plastic anisotropy, flow behavior and stretch flangeability of a TWIP steel sheet sample. During the hole expansion tests, strain distribution was measured. Finite element simulations with different yield criteria, von Mises, Hill 1948 and Yld2000-2d, were carried out using ABAQUS. Experimental and predicted hole radii and thickness strain right after the fracture, were compared. It was shown that, no matter which yield criterion was used in the simulation, the predicted hole radii were always much larger than experimental radii, and correspondingly, the predicted thickness strains were smaller than those in experiments. Moreover, the plastic anisotropy exhibiting in the experimental hole radii can not be reproduced by the anisotropic yield criteria, but it seems that the variation of thickness strain along hole periphery could be roughly predicted. The results also show that the thickness strain distribution was nearly homogenous from hole edge to punch shoulder in the experiment and simulations. In addition, the comparison of major strain distribution between experimental and numerical shows that, even before reaching the maximum punch force, the strains were also overpredicted. Therefore, more work is needed to understand the process and improve the model prediction of the hole expansion test.

ACKNOWLEDGMENTS

The authors are grateful to Dr Jeong Whan YOON for providing his ABAQUS UMAT of Yld2000-2d yield criterion.

REFERENCES

1. S. B. Lee, Y. R. Cho, K. G. Chin, *POSCO Technical Report*10 (1), 2007, pp. 104-11.5
2. H. Takuda, K. Mori, H. Fujimoto, N. Hatta, *Journal of Materials Processing Technology* **92-93**, 433-438 (1999).
3. R. von Mises, *Göttinger Nachrichten Math. Phys. Klasse*, 1913, pp. 582-592.
4. R. Hill, *Proc. Roy. Soc. London* **A193**, 281-297 (1948).
5. F. Barlat, J. C. Brem, J. W. Yoon, K. Chung, R. E. Dick, D. J. Lege, F. Pourboghart, S. H. Choi, E. Chu, *International Journal of Plasticity***19**, 1297-1319 (2003).
6. L. Xu, F. Barlat, Proceeding of 9th International Conference on Technology of Plasticity, Gyeongju, Republic of Korea, 2008, pp. 2312-2317.
7. R. J. Comstock, Jr., D. K. Scherrer, R. D. Adamczyk, *Journal of Materials Engineering and Performance* **15**, 675-683 (2006).
8. W. F. Hosford, Proc. 7th North American Metalworking Conf SME, Dearborn, MI, 1979, pp. 191-197.